THE RAYLEIGH-LAMB WAVE PROPAGATION IN DIELECTRIC ELASTOMER LAYERS SUBJECTED TO LARGE DEFORMATIONS

GAL SHMUEL[†], MASSIMILIANO GEI [‡] AND GAL DEBOTTON [†,§]

[†] THE PEARLSTONE CENTER FOR AERONAUTICAL STUDIES,
DEPARTMENT OF MECHANICAL ENGINEERING,
BEN-GURION UNIVERSITY,
BEER-SHEVA 84105, ISRAEL.

[‡] DEPARTMENT OF MECHANICAL AND STRUCTURAL ENGINEERING,
UNIVERSITY OF TRENTO,
VIA MESIANO 77, 38123 TRENTO, ITALY.

[§] DEPARTMENT OF BIOMEDICAL ENGINEERING,
BEN-GURION UNIVERSITY,
BEER-SHEVA 84105, ISRAEL.

ABSTRACT. The propagation of waves in soft dielectric elastomer layers is investigated. To this end incremental motions superimposed on homogeneous finite deformations induced by bias electric fields and pre-stretch are determined. First we examine the case of mechanically traction-free layer, which is an extension of the Rayleigh-Lamb problem in the purely elastic case. Two other loading configurations are accounted for too. Subsequently, numerical examples for the dispersion relations are evaluated for a dielectric solid governed by an augmented neo-Hookean strain energy. It is found that the the phase speeds and frequencies strongly depend on the electric excitation and pre-stretch. These findings lend themselves at the possibility of controlling the propagation velocity as well as filtering particular frequencies with suitable choices of the electric bias field.

Keywords: dielectric elastomers; electroelastic waves; finite deformations; soft actuators; non-linear electroelasticity.

1. INTRODUCTION

The goal of this work is to investigate the propagation of electromechanical induced waves in a dielectric elastomer (DE) layer subjected to finite deformations. In the purely elastic case the first solution for surface waves based on the exact equations of (2D) elasticity was introduced by Lord Rayleigh in 1887, who determined the so-called Rayleigh waves. This work was later extended for propagation of waves in elastic plates by Lord Rayleigh (1889) himself and Lamb (1889).

Here we extend the Rayleigh-Lamb problem and account for incremental motions superimposed on finite deformations in dielectric media, and investigate how these are influenced by the presence of external electric field and pre-stretch.

When subjected to an electric field electroactive polymers (EAPs) deform and both their mechanical and electrical properties are modified. In contrast to piezoelectric ceramics, DEs are capable of undergoing large deformations, a property that entitled them the name "artificial muscles". Moreover, while in piezoelectricity the electromechanical coupling is linear, in DEs the mechanical field depends quadratically on the electric fields. A proper theory, which accounts for the aforementioned coupling and captures the ability of the material to undergo finite strains is therefore required. The foundations of this nonlinear electroelastic theory are summarized in the pioneering works of Toupin (1956) and Eringen (1963) for the static case. These contributions were later extended by Toupin (1963) to account for the dynamics of these elastic dielectrics. A comprehensive summary can be found in monographs by Eringen and Maugin (1990) and Kovetz (2000). Due to the development of new materials that admit this coupled behavior, thus branching toward a window of new applications (e.g., Pelrine et al., 2000, Bar-Cohen, 2002 and Carpi and Smela, 2009), the interest in these electroelastodynamic theories revived recently and the coupled electromechanical theory was revisited recently (e.g., McMeeking and Landis, 2005; Dorfmann and Ogden, 2005; Ericksen, 2007; Suo et al., 2008). The foregoing works and their extension to the domain of soft dielectric composites by deBotton et al. (2007) and Bertoldi and Gei (2011), differ in their constitutive formulations, the choice of the independent variables, the resultant electrostatic stress-like tensors and electric body-like forces. For a review of the diverse formulations of the constitutive laws and governing equations the reader is referred to Bustamante et al. (2009). Among the various approaches we recall the formulation proposed by Dorfmann and Ogden (2005) for the static case, and its extension to dynamics by Dorfmann and Ogden (2010). In these works the concept of 'total' stress tensor that is derived from a 'total' or 'augmented' energy-density function was employed. In this work we follow the framework proposed by the latter.

In contrast with the relatively large body of theoretical works that are available, only a few boundary-value problems (BVP) were solved in the context of the dynamic behavior of electromechanically coupled EAPs. One of the first contributions in the field of piezoelectricity was made by Tiersten (1963a), who examined the thickness vibrations of an infinite piezoelectric plate induced by alternating voltage at the surface electrodes, and later solved the corresponding problem of wave propagation (Tiersten, 1963b). To the best of the authors knowledge, while for piezoelectric media solutions for BVP accounting for the influence of pre-strain and bias field are available (see review article by Yang and Hu, 2004), analogue developments in the context of dielectrics were considered

by Mockensturm and Goulbourne (2006) and Zhu et al. (2010), who examined the dynamic behavior of dielectric elastomer balloons, and by Dorfmann and Ogden (2010) who studied the problem of propagation of Rayleigh surface waves in a dielectric half-space. Herein we continue along the path of the latter contribution and consider the extension of the Rayleigh-Lamb wave propagation problem to finitely deformed dielectric layers subjected to coupled electromechanical loading.

The work is composed as follows. In section 2 the theory of finite electroelastodynamics is summarized. The equations for incremental motions superimposed on finite deformations are outlined in section 3. Specific finite deformations that correspond to three different loading configurations are considered in section 4 for a layer whose behavior is characterized by a particular augmented energy-density function (AEDF), namely the *incompressible dielectric neo-Hookean* model (DH). Next, the extension of the Rayleigh-Lamb dispersion relation for a DH layer is introduced in section 5. An analysis of the dispersion relation is carried out in section 6, and the effects of the bias electrostatic field and pre-stretch are investigated for the three loading configurations. The main conclusions and observations are summarized in section 7.

2. Finite electroelasticity

Let $\chi : \Omega_0 \times \mathscr{I} \to \Omega \subset \mathbb{R}^3$ describe the motion of a material point $\mathbf{X}$ from a reference configuration of a body Ω_0, with a boundary $\partial\Omega_0$, to its current configuration Ω, with boundary $\partial\Omega$, by $\mathbf{x} = \chi(\mathbf{X}, t)$, where $\mathscr{I}$ is a time interval. The domain of the space surrounding the body is $\mathbb{R}^3 \backslash \Omega$ and is assumed to be vacuum. The corresponding velocity and acceleration are denoted by $\mathbf{v} = \chi_{,t}$ and $\mathbf{a} = \chi_{,tt}$, respectively, while the deformation gradient is $\mathbf{F} = \frac{\partial \chi}{\partial \mathbf{X}} = \nabla_{\mathbf{X}} \chi$, and where due to the material impenetrability $J \equiv \det(\mathbf{F}) > 0$. Vectors between two infinitesimally close points are related through $\mathrm{d}\mathbf{x} = \mathbf{F}\mathrm{d}\mathbf{X}$, whereas area elements are transformed via Nanson's formula $\mathbf{N}\mathrm{d}A = \frac{1}{J}\mathbf{F}^{\mathrm{T}}\mathbf{n}\mathrm{d}a$. The volume ratio between an infinitesimal volume element $\mathrm{d}v$ in the deformed configuration, and its counterpart in the reference $\mathrm{d}V$ is given by $\mathrm{d}v = J\mathrm{d}V$. As measures of the deformation the right and left Cauchy-Green strain tensors $\mathbf{C} = \mathbf{F}^{\mathrm{T}}\mathbf{F}$ and $\mathbf{b} = \mathbf{F}\mathbf{F}^{\mathrm{T}}$ are used.

Let $\mathbf{e}$ denote the electric field in the current configuration. Commonly the electric field is given by means of a gradient of a scalar field, namely the electrostatic potential. The induced electric displacement field $\mathbf{d}$ is related to the electric field in free space via the vacuum permittivity ε_0 such that $\mathbf{d} = \varepsilon_0 \mathbf{e}$. In dielectric media an appropriate constitutive law specifies the relationship between these fields. Generally, this connection can be non-linear and anisotropic.

The balance of linear momentum is

$$\nabla \cdot \boldsymbol{\sigma} = \rho \mathbf{a}, \tag{2.1}$$

where σ is the 'total' stress tensor, and ρ is the material mass density. The balance of angular momentum implies that σ is symmetric. Note that σ consists of both mechanical and electrical contributions, such that the traction $\mathbf{t}$ on a deformed area element can be written as $\sigma\mathbf{n}$ where $\mathbf{n}$ is unit vector normal to $\partial\Omega$. On the boundary of the material we postulate a separation of the traction into the sum of a mechanical traction $\mathbf{t}_m$ which is a prescribed data, and an electrical traction $\mathbf{t}_e$ which is induced by the external electric field.

Assuming no free body charge (ideal dielectric), Gauss' law reads

$$\nabla \cdot \mathbf{d} = 0. \tag{2.2}$$

Under a quasi-electrostatic approximation, appropriate when for the same frequency the length of the waves under consideration are shorter than the electromagnetic waves, Faraday's law states that the electric field is curl-free, i.e.,

$$\nabla \times \mathbf{e} = \mathbf{0}, \tag{2.3}$$

thus enabling the usage of the aforementioned electrostatic potential.

Taking into account fields outside the material, which henceforth will be identified by a star superscript, the following jump conditions should be satisfied across $\partial\Omega$, namely

$$[[\sigma]]\,\mathbf{n} = \mathbf{t}_m, \qquad [[\mathbf{d}]] \cdot \mathbf{n} = -w_e, \qquad [[\mathbf{e}]] \times \mathbf{n} = \mathbf{0}, \tag{2.4}$$

where w_e is the surface charge density, and the notation $[[\bullet]] = (\bullet) - (\bullet)^\star$ is used for the difference between fields inside and outside of the material. The outer fields are related by

$$\mathbf{d}^\star = \varepsilon_0 \mathbf{e}^\star, \tag{2.5}$$

$$\sigma^\star = \varepsilon_0 \left[\mathbf{e}^\star \otimes \mathbf{e}^\star - \frac{1}{2} (\mathbf{e}^\star \cdot \mathbf{e}^\star)\, \mathbf{I} \right], \tag{2.6}$$

where $\mathbf{I}$ is the identity tensor. Herein we identify the electrical traction $\mathbf{t}_e$ as the consequence of the external stress $\sigma^\star$, namely the Maxwell stress, such that $\mathbf{t}_e = \sigma^\star \mathbf{n}$. In the surrounding space outside the material $\mathbf{d}^\star$ and $\mathbf{e}^\star$ must satisfy Eqs. (2.2)-(2.3), which reduce to Laplace equation of the electrostatic potential. As a consequence the Maxwell stress is divergence-free.

The foregoing balance and jump equations can be recast in a Lagrangian formulation with the appropriate *pull-back* operations. Specifically, we have that

$$\mathbf{P} = J\sigma\mathbf{F}^{-\mathrm{T}}, \qquad \mathbf{D} = J\mathbf{F}^{-1}\mathbf{d}, \qquad \mathbf{E} = \mathbf{F}^{\mathrm{T}}\mathbf{e}, \tag{2.7}$$

for the 'total' first Piola-Kirchhoff stress, Lagrangian electric displacement and electric field, respectively (e.g., Dorfmann and Ogden, 2005). The corresponding balance equations are

$$\nabla_{\mathbf{X}} \cdot \mathbf{P} = \rho_L \mathbf{a}, \qquad \nabla_{\mathbf{X}} \cdot \mathbf{D} = 0, \qquad \nabla_{\mathbf{X}} \times \mathbf{E} = \mathbf{0}, \tag{2.8}$$

where $\rho_L = J\rho$ is the density of the material in the reference configuration. The jump conditions across the boundary $\partial\Omega_0$ read

$$[[\mathbf{P}]]\,\mathbf{N} = \mathbf{t}_M, \qquad [[\mathbf{D}]] \cdot \mathbf{N} = -w_E, \qquad [[\mathbf{E}]] \times \mathbf{N} = \mathbf{0}, \tag{2.9}$$

where $\mathbf{t}_M \mathrm{d}A = \mathbf{t}_m \mathrm{d}a$, $w_E \mathrm{d}A = w_e \mathrm{d}a$ and $\mathbf{N}$ is a unit outward normal to $\partial\Omega_0$.

Following Dorfmann and Ogden (2005), the 'total' first Piola-Kirchhoff stress and the Lagrangian electric field are given in terms of an *augmented* energy-density function Ψ (AEDF) with the independent variables $\mathbf{F}$ and $\mathbf{D}$, such that

$$\mathbf{P} = \frac{\partial \Psi}{\partial \mathbf{F}}, \quad \mathbf{E} = \frac{\partial \Psi}{\partial \mathbf{D}}. \tag{2.10}$$

For an incompressible material a Lagrange multiplier p is introduced, which is a workless reaction to the kinematic constraint such that

$$\mathbf{P} = \frac{\partial \Psi}{\partial \mathbf{F}} - p\mathbf{F}^{-\mathrm{T}}. \tag{2.11}$$

The latter can be determined only from the equilibrium equations and the boundary conditions.

3. Small fields superimposed on finite deformations

Recent experiments reveal how pre-stretching of dielectric elastomers enhances properties such as the actuation strain (Pelrine et al., 2000) and breakdown strength (Plante and Dubowsky, 2006). A thorough investigation of the subject was recently done by Kofod (2008). Motivated by these findings, we address the response of pre-stretched dielectric elastomers to incremental deformations.

Following the formulation given in Dorfmann and Ogden (2010), we consider infinitesimal time-dependent elastic displacement and electric displacement increments $\dot{\mathbf{x}} = \dot{\chi}(\mathbf{X},t)$ and $\dot{\mathbf{D}}(\mathbf{X},t)$, respectively, superimposed on the foregoing static configuration Ω reached via $\chi(\mathbf{X})$. Herein and throughout this work a superposed dot will denote the incremental quantities. The corresponding balance laws can be formulated in terms of Eulerian quantities, namely

$$\nabla \cdot \Sigma = \rho \dot{\mathbf{x}}_{,tt}, \qquad \nabla \cdot \check{\mathbf{d}} = 0, \qquad \nabla \times \check{\mathbf{e}} = \mathbf{0}, \tag{3.1}$$

such that Σ $\check{\mathbf{d}}$ and $\check{\mathbf{e}}$ are, respectively, the *push-forwards* of the increments in the total first Piola-Kirchhoff stress, the Lagrangian electric displacement and the electric field determined via the

inverse of the transformations given in Eq. (2.7). Next, upon linearization, the incremental constitutive equations for an incompressible material are

$$\Sigma = \mathscr{C}\mathbf{h} + p\mathbf{h}^{\mathrm{T}} - \dot{p}\mathbf{I} + \mathscr{B}\check{\mathbf{d}}, \tag{3.2}$$

$$\check{\mathbf{e}} = \mathscr{B}^{\mathrm{T}}\mathbf{h} + \mathscr{A}\check{\mathbf{d}}, \tag{3.3}$$

where $\left(\mathscr{B}^{\mathrm{T}}\mathbf{h}\right)_k = \mathscr{B}_{ijk}h_{ij}$. For a compressible material Eq. (3.2) is to be taken with $p \equiv \dot{p} \equiv 0$. Herein $\mathbf{h} = \nabla\dot{\mathbf{x}}$ is the displacement gradient and

$$\mathscr{A}_{ij} = JF^{-1}_{\alpha i}F^{-1}_{\beta j}\mathscr{A}_{0\alpha\beta}, \qquad \mathscr{B}_{ijk} = F_{j\alpha}F^{-1}_{\beta k}\mathscr{B}_{0i\alpha\beta}, \qquad \mathscr{C}_{ijkl} = \frac{1}{J}F_{j\alpha}F_{l\beta}\mathscr{C}_{0i\alpha k\beta}, \tag{3.4}$$

are the push-forwards of the referential electric, electroelastic, and elasticity tensors, respectively. The latter are defined by

$$\mathscr{A}_{0\alpha\beta} = \frac{\partial^2\Psi}{\partial D_\alpha \partial D_\beta}, \qquad \mathscr{B}_{0i\alpha\beta} = \frac{\partial^2\Psi}{\partial F_{i\alpha}\partial D_\beta}, \qquad \mathscr{C}_{0i\alpha k\beta} = \frac{\partial^2\Psi}{\partial F_{i\alpha}\partial F_{k\beta}}. \tag{3.5}$$

Similarly, the incremental outer fields are

$$\dot{\mathbf{d}}^\star = \varepsilon_0\dot{\mathbf{e}}^\star, \tag{3.6}$$

$$\dot{\boldsymbol{\sigma}}^\star = \varepsilon_0\left[\dot{\mathbf{e}}^\star\otimes\mathbf{e}^\star + \mathbf{e}^\star\otimes\dot{\mathbf{e}}^\star - \left(\mathbf{e}^\star\cdot\dot{\mathbf{e}}^\star\right)\mathbf{I}\right], \tag{3.7}$$

where $\dot{\mathbf{d}}^\star$ and $\dot{\mathbf{e}}^\star$ are to satisfy Eqs. (2.2)-(2.3), hence $\dot{\boldsymbol{\sigma}}^\star$ is identically divergence-free.

Utilizing several kinematic relations (see Dorfmann and Ogden, 2010) the corresponding jump conditions are

$$\left[\Sigma - \dot{\boldsymbol{\sigma}}^\star + \boldsymbol{\sigma}^\star\mathbf{h}^{\mathrm{T}} - (\nabla\cdot\dot{\mathbf{x}})\,\boldsymbol{\sigma}^\star\right]\mathbf{n} = \check{\mathbf{t}}_m, \tag{3.8}$$

$$\left[\check{\mathbf{d}} - \dot{\mathbf{d}}^\star - (\nabla\cdot\dot{\mathbf{x}})\,\mathbf{d}^\star + \mathbf{h}\mathbf{d}^\star\right]\cdot\mathbf{n} = -\check{w}_e, \tag{3.9}$$

$$\left[\check{\mathbf{e}} - \dot{\mathbf{e}}^\star - \mathbf{h}^{\mathrm{T}}\mathbf{e}^\star\right]\times\mathbf{n} = \mathbf{0}, \tag{3.10}$$

where the quantities $\check{\mathbf{t}}_m$ and $\check{w}_e$ are defined by $\check{\mathbf{t}}_m\mathrm{d}a = \dot{\mathbf{t}}_M\mathrm{d}A$ and $\check{w}_e\mathrm{d}a = \dot{w}_E\mathrm{d}A$.

4. Incompressible dielectric neo-Hookean layer subjected to transverse bias field

We recall that the constitutive laws in terms of the AEDF has the deformation gradient and the electric displacement field as its independent variables. Whenever the material is isotropic its symmetry can be exploited, and the dependency of the AEDF on $\mathbf{F}$ and $\mathbf{D}$ is reduced to the appropriate invariants of $\mathbf{C}$ and $\mathbf{D}\otimes\mathbf{D}$, namely

$$I_1 = \mathrm{tr}\,(\mathbf{C}) = \mathbf{C}:\mathbf{I}, \quad I_2 = \tfrac{1}{2}\left(I_1^2 - \mathbf{C}:\mathbf{C}\right), \quad I_3 = \det(\mathbf{C}) = J^2, \tag{4.1}$$

and

$$I_{4e} = \mathrm{tr}\,(\mathbf{D}\otimes\mathbf{D})\,, \quad I_{5e} = \mathbf{C} : (\mathbf{D}\otimes\mathbf{D})\,, \quad I_{6e} = \mathbf{C}^2 : (\mathbf{D}\otimes\mathbf{D})\,. \tag{4.2}$$

Thus, we consider the AEDF

$$\Psi_{DH}\,(I_1, I_{5e}) = \frac{\mu}{2}\,(I_1 - 3) + \frac{1}{2\varepsilon} I_{5e}, \tag{4.3}$$

where μ is the shear modulus and ε is the material permittivity that equals the vacuum permittivity ε_0 times the material relative permittivity ε_r. This model recovers a neo-Hookean behavior in a purely elastic case, as well as the simple isotropic linear relation $\mathbf{d} = \varepsilon\mathbf{e}$ between the current displacement and electric field. Henceforth we refer to Eq. (4.3) as the *incompressible dielectric neo-Hookean* model (DH). Throughout this work the material behavior is assumed to be governed by the DH model. The corresponding total stress is

$$\sigma = \mu\mathbf{b} + \frac{1}{\varepsilon}\mathbf{d}\otimes\mathbf{d} - p\mathbf{I}, \tag{4.4}$$

where, in component form, the constitutive tensors $\mathscr{A}$, $\mathscr{B}$, and $\mathscr{C}$ are

$$\mathscr{A}_{ij} = \frac{1}{\varepsilon}\delta_{ij}, \qquad \mathscr{B}_{ijk} = \tfrac{1}{\varepsilon}\left(\delta_{ik}d_j + d_i\delta_{jk}\right), \qquad \mathscr{C}_{ijkl} = \mu\,\delta_{ik}b_{jl} + \frac{1}{\varepsilon}\delta_{ik}d_j d_l. \tag{4.5}$$

Consider a Cartesian coordinate system with unit vectors $\mathbf{i_1}, \mathbf{i_2}$ and $\mathbf{i_3}$ along the x_1, x_2 and x_3 axes, respectively. Let a layer governed by the DH model be infinitely long along the x_1-axis with a thickness $2h$ along the x_2-axis. Assuming a plane-strain configuration there is no deformation along the x_3-axis and the fields being independent of x_3. An electric displacement field is applied to the layer along its thickness. In the current configuration this field is given by $\mathbf{d} = d_2\mathbf{i_2}$, and the corresponding electric field equals the voltage difference between the electrodes divided by $2h$. The resultant deformation in terms of a homogeneous diagonal deformation gradient $\mathrm{F} = \mathrm{diag}\left[\lambda, \lambda^{-1}, 1\right]$, is related to the stress via

$$\sigma_{11} = \mu\lambda^2 - p, \qquad \sigma_{22} = \tfrac{\mu}{\lambda^2} + \tfrac{1}{\varepsilon}d_2^2 - p. \tag{4.6}$$

Specialization of the in-plane components of Eq. (3.5) for the considered deformation gives

$$\mathscr{A}_{11} = \mathscr{A}_{22} = \frac{1}{\varepsilon}, \tag{4.7}$$

$$\mathscr{B}_{121} = \mathscr{B}_{211} = \frac{1}{2}\mathscr{B}_{222} = \frac{1}{\varepsilon}d_2, \tag{4.8}$$

$$\mathscr{C}_{1111} = \mathscr{C}_{2121} = \mu\lambda^2, \tag{4.9}$$

$$\mathscr{C}_{1212} = \mathscr{C}_{2222} = \frac{\mu}{\lambda^2} + \frac{1}{\varepsilon}d_2^2. \tag{4.10}$$

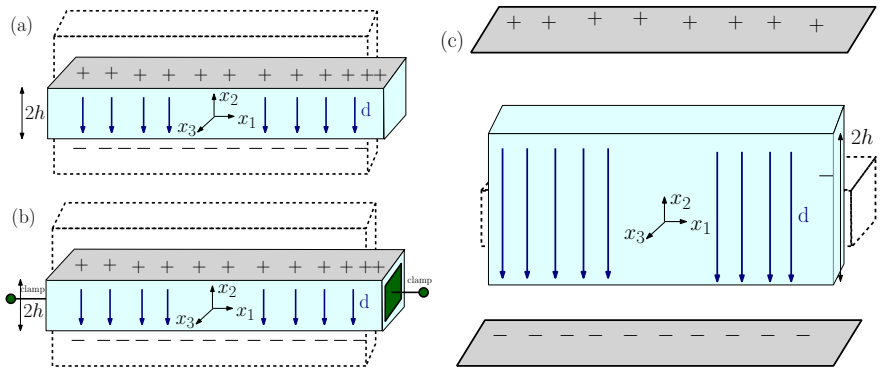

FIGURE 4.1. Illustration of (a) path A: expansion-free loading, (b) path B: initially pre-stretched layer, and (c) path C: a layer immersed in electric field.

Wave propagation and vibrations of the layer are addressed for the following three fundamental loading paths.

Path A: expansion-free finite loading. The layer having its top and bottom surfaces $x_2 = \pm h$ coated with soft electrodes and mechanically traction free ($\mathbf{t}_m = \mathbf{0}$). It is also free to expand along the x_1-axis (Fig. 4.1a). From the traction-free boundary conditions simple connections between the stretch, the pressure and the Lagrangian electric displacement field $\mathbf{D} = \lambda \mathbf{d}$ are obtained, namely

$$\lambda = \left(1 + \hat{D}^2\right)^{1/4}, \qquad p = \mu \left(1 + \hat{D}^2\right)^{1/2}, \tag{4.11}$$

where $\hat{D} = D_2/\sqrt{\mu\varepsilon}$. Note that due to the symmetry of the problem the electric fields along with the Maxwell stress outside the layer vanish. The surface charge w_E is evaluated via Eq. (2.9), recalling that $\mathbf{d}^\star = \mathbf{0}$.

Path B: initially pre-stretched layer. Once again the surfaces $x_2 = \pm h$ are coated with electrodes and are free of mechanical traction. The layer is first pre-stretched along the x_1-axis to $\lambda = \tilde{\lambda}$, and then clamped (Fig. 4.1b). Subsequently, an electric displacement field is applied, while the longitudinal stretch is kept constant. The pressure is given in terms of the pre-stretch and the electric displacement field as

$$p = \mu \left(\frac{1}{\tilde{\lambda}^2} + \hat{d}^2 \right), \tag{4.12}$$

where $\hat{d} = d_2/\sqrt{\mu\varepsilon}$. The resultant pre-stress is obtained via Eq. (4.6). Again, the electric fields and the Maxwell stress outside the layer vanish. The surface charge w_e is evaluated via Eq. (2.4), having that $\mathbf{d}^\star = \mathbf{0}$.

Path C: a layer immersed in electric field. The layer is immersed in a pre-existing electric field. The surfaces are free of mechanical traction. The absence of the electrodes on the surfaces implies that $w_E = 0$, where the pressure and the stretch are determined via the corresponding jump

conditions to yield

$$\lambda = \left(1 - \hat{D}^2\left(\varepsilon_r - 1\right)\right)^{1/4}, \qquad p = \tfrac{\mu\hat{D}^2}{2\lambda^2}\left(1+\lambda^4\right). \tag{4.13}$$

We note that when deriving the solution it was assumed the electric field is homogeneous outside the layer, neglecting fringing effects. Thus, this solution is by no means exact, and serves only as a qualitative result. Eq. (4.13a) reveals that the layer contracts along the x_1-axis and expands along the direction of the electric displacement, contrary to the situation in path A.

5. Wave propagation in dielectric layers

We determine next the mechanical and electrical waves due to harmonic excitation along the x_1-axis superimposed on the deformed configurations described previously. Following Dorfmann and Ogden (2010), the incremental equations of motion (3.1a) read

$$\left(\mu\lambda^2 + p\right)h_{11,1} - \dot{p}_{,1} + \left(\frac{\mu}{\lambda^2} + \frac{1}{\varepsilon}d_2^2\right)h_{12,2} + ph_{21,2} + \frac{1}{\varepsilon}d_2\check{d}_{1,2} = \rho\dot{x}_{1,tt}, \tag{5.1}$$

$$\left(\mu\lambda^2 + p\right)h_{21,1} + ph_{12,1} + \frac{1}{\varepsilon}d_2\check{d}_{1,1} + \left(\frac{\mu}{\lambda^2} + \frac{1}{\varepsilon}d_2^2 + p\right)h_{22,2} - \dot{p}_{,2} + 2\frac{1}{\varepsilon}d_2\check{d}_{2,2} = \rho\dot{x}_{2,tt}, \tag{5.2}$$

while the incremental Faraday's equation (3.1c) is

$$\frac{1}{\varepsilon}d_2\left(h_{12,2} + h_{21,2}\right) + \frac{1}{\varepsilon}\check{d}_{1,2} - 2\frac{1}{\varepsilon}d_2h_{22,1} - \frac{1}{\varepsilon}\check{d}_{2,1} = 0. \tag{5.3}$$

The motion has to satisfy the incompressibility constraint and Gauss' equation, namely

$$h_{11} + h_{22} = 0, \qquad \check{d}_{1,1} + \check{d}_{2,2} = 0, \tag{5.4}$$

which motivate the use of stream functions $\phi\left(x_1, x_2, t\right)$ and $\varphi\left(x_1, x_2, t\right)$ such that

$$\dot{x}_1 = \phi_{,2}, \quad \dot{x}_2 = -\phi_{,1}, \qquad \check{d}_1 = \varphi_{,2}, \qquad \check{d}_2 = -\varphi_{,1}. \tag{5.5}$$

Normalization by $\mu\lambda^2$, followed by differentiation of Eqs. (5.1) and (5.2) with respect to x_2 and x_1, respectively, and then subtraction of the latter form the former results in the coupled equation

$$\phi_{,1111} + \left(1 + \frac{1+\hat{D}^2}{\lambda^4}\right)\phi_{,1122} + \frac{1+\hat{D}^2}{\lambda^4}\phi_{,2222} + \frac{\hat{D}}{\lambda^3\sqrt{\mu\varepsilon}}\left(\varphi_{,112} + \varphi_{,222}\right) = \frac{1}{\lambda^2}\frac{\rho}{\mu}\left(\phi_{,11} + \phi_{,22}\right)_{,tt}, \tag{5.6}$$

After multiplying Eq. (5.3) by $\lambda\sqrt{\frac{\varepsilon}{\mu}}$ it may be rewritten in the form

$$\hat{D}\left(\phi_{,112} + \phi_{,222}\right) + \frac{\lambda}{\sqrt{\mu\varepsilon}}\left(\varphi_{,11} + \varphi_{,22}\right) \;=\; 0. \tag{5.7}$$

The last two equations constitute a system of two coupled equations for the stream functions ϕ and φ. A solution is feasible once the current stretch λ and the dimensionless nominal electric

displacement $\hat{\mathrm{D}}$ are prescribed in addition to the density ρ and shear modulus μ of the layer. We recall that while for the paths A and C the quantities $\hat{\mathrm{D}}$ and λ are uniquely related via Eqs. (4.11a) and (4.13a), respectively, they are independent for path B. Also note that the quantity $1/\sqrt{\mu\varepsilon}$ can be integrated into the amplitude of the stream function φ.

Next we assume a solution with time-dependency in the form $e^{-i\omega t}$ and a periodicity along the x_1-axis in the form e^{ikx_1}, where ω is the angular frequency and k is the associated wavenumber, such that the wave velocity is $c=\omega/k$. Thus, traveling waves solutions in the form

$$\phi = Ae^{kqx_2}e^{ik(x_1-ct)}, \qquad \varphi = kBe^{kqx_2}e^{ik(x_1-ct)}, \tag{5.8}$$

are sought, where the appropriate values of q are to be found from the governing equations. Insertion of Eq. (5.8) into Eqs. (5.6)-(5.7) yields the following system of two linear homogeneous equations in A and B, namely

$$\left(q^2-1\right)\left(\frac{\rho}{\mu}c^2+q^2\frac{1+\hat{D}^2}{\lambda^2}-\lambda^2\right)A+\left(q^2-1\right)q\frac{1}{\lambda}\hat{D}\hat{B} = 0, \tag{5.9}$$

$$q\left(q^2-1\right)\hat{D}A+\left(q^2-1\right)\lambda\hat{B} = 0, \tag{5.10}$$

where $\hat{B}=B/\sqrt{\mu\varepsilon}$. A non-trivial solution is possible for values of q for which the determinant of the coefficients of A and B vanish. This leads to a bi-cubic equation in q. The six roots include two repeated ones, namely $q_1=q_2=1$ and $q_3=q_4=-1$, along with roots $q_5=-q_6=\lambda\left(\lambda^2-\frac{\rho}{\mu}c^2\right)^{1/2}$.

An interesting case arises if $c^2=\lambda^2\frac{\mu}{\rho}$, that is the square of the speed of a bulk shear wave in an isotropic elastic medium subjected to a finite deformation propagating along the axis with principal stretch λ. In this case $q_5=q_6=0$, and the corresponding solution is associated with propagation of waves parallel to the boundary along the x_1-axis. As observed by Dorfmann and Ogden (2010) for the half-space case, the associated stream functions vanish as expected since an in-plane bulk shear wave cannot propagate in this manner.

Usually, the general solutions for ϕ and φ are obtained as a linear combination of the roots in the form of

$$\phi=\sum_{n=1}^{6}A_ne^{kq_nx_2}e^{ik(x_1-ct)}, \qquad \varphi=\sum_{n=1}^{6}B_ne^{kq_nx_2}e^{ik(x_1-ct)}. \tag{5.11}$$

However, a somewhat different structure of the solution is required for the DH model. For the general case when the constitutive law involves I_{4e}, a full coupling between the mechanical and electric equations is expected (see Dorfmann and Ogden, 2010), and hence dependency between A_n and B_n exists for all n. However, for the specific constitutive behavior considered here we find that for the roots $\{q_n\}$, $n=1,..,4$, the coefficients associated with $A_1,...,A_4,B_1,...,B_4$ in the

counter diagonal of the coefficients matrix vanishes. Mathematically, this implies that the constants $A_1,...,A_4$ and $B_1,...,B_4$ are independent. Physically, this hints at the possibility of propagation of elastic waves without excitation of the accompanying electric waves. Thus, the associated solutions for ϕ and φ of these roots are not to be taken as multiple. The coupling between the coefficients still holds when q_5 and q_6 are considered, giving a relation between A_5 and B_5, and between A_6 and B_6. This relation is obtained by substituting q_5 and q_6 into Eq. (5.9), or equivalently into Eq. (5.10). Hence, the solutions sought for the DH layer are

$$\phi = \sum_{n=1,3,5,6} A_n e^{kq_n x_2} e^{ik(x_1-ct)}, \qquad \varphi = \sum_{n=1,3,5,6} kB_n e^{kq_n x_2} e^{ik(x_1-ct)}, \tag{5.12}$$

where the six unknowns are A_1, A_3, A_5, A_6, B_1 and B_3, while B_5 and B_6 are functions of A_5 and A_6.

We note that once the layer is excited the symmetry in paths A and B is broken. Accordingly, for all paths the incremental exterior fields must be accounted for. Motivated by the need to satisfy a decaying condition at $x_2 \to \pm\infty$ along with Laplace's equation outside the material, we consider the following stream functions

$$\psi^\star = C_1 ike^{-kx_2} e^{ik(x_1-ct)} \text{ at } x_2 > h, \tag{5.13}$$

$$\vartheta^\star = C_2 ike^{kx_2} e^{ik(x_1-ct)} \text{ at } x_2 < -h, \tag{5.14}$$

such that the electric field components are given by

$$\dot{e}_1^\star = \begin{cases} -\psi_{,1}^\star & x_2 > h \\ -\vartheta_{,1}^\star & x_2 < -h \end{cases}, \qquad \dot{e}_2^\star = \begin{cases} -\psi_{,2}^\star & x_2 > h \\ -\vartheta_{,2}^\star & x_2 < -h \end{cases}. \tag{5.15}$$

In summary, we end up with a set of eight constants to be determined, namely $\{A_n\}$, $n = 1,3,5,6$, $\{B_n\}, n = 1,3$ and C_1, C_2 via the appropriate jump conditions. Henceforth we distinguish the solutions of paths A and B from the one along path C.

Paths A and B. The Maxwell stress, and as a consequence of Eq. (3.7), its increment vanish outside the layer ($\sigma^\star = \dot{\sigma}^\star = \mathbf{0}$). Further, the surfaces remain traction-free and hence the jump in the stress according to Eq. (3.8) becomes

$$\Sigma_{22} = 0 \text{ at } x_2 = \pm h, \tag{5.16}$$

$$\Sigma_{12} = 0 \text{ at } x_2 = \pm h, \tag{5.17}$$

where

$$\Sigma_{22} = -\left(\frac{\mu}{\lambda^2} + \frac{1}{\varepsilon}d_2^2 + p\right)\phi_{,12} - \dot{p} - 2\frac{1}{\varepsilon}d_2\varphi_{,1}, \tag{5.18}$$

$$\Sigma_{12} = \left(\frac{\mu}{\lambda^2} + \frac{1}{\varepsilon}d_2^2\right)\phi_{,22} - p\phi_{,11} + \frac{1}{\varepsilon}d_2\varphi_{,2}. \tag{5.19}$$

The solution sought for the incremental pressure is

$$\dot{p}(x_1, x_2, t) = k\left(P_1 e^{kq_1 x_2} + P_3 e^{kq_3 x_2}\right) e^{ik(x_1 - ct)}, \tag{5.20}$$

where P_1 and P_3 are determined via Eqs. (5.1)-(5.2).

As the electrodes surface charge is fixed we have that $\dot{w}_e = 0$, and the corresponding jump condition in Eq. (3.9) becomes

$$\dot{d}_2^\star - \check{d}_2 \quad = \quad 0 \text{ at } x_2 = \pm h, \tag{5.21}$$

where $\dot{d}_2^\star = \varepsilon_0 \dot{e}_2^\star$. The jump in Eq. (3.10) is

$$\dot{e}_1^\star - \check{e}_1 = 0 \text{ at } x_2 = \pm h, \tag{5.22}$$

where $\check{e}_1 = \frac{1}{\varepsilon}d_2(\phi_{,22} - \phi_{,11}) + \frac{1}{\varepsilon}\varphi_{,2}$. Note that while the increment in the Maxwell stress is zero as discussed before, Eqs. (5.21)-(5.22) state that $\dot{\mathbf{d}}^\star$ and $\dot{\mathbf{e}}^\star$ do not vanish.

Path C. Along this path the Maxwell stress and its increment do not vanish outside the layer, yielding the following form of Eq. (3.8)

$$\Sigma_{22} - \dot{\sigma}^\star{}_{22} + \sigma_{22}^\star h_{22} \quad = \quad 0 \text{ at } x_2 = \pm h, \tag{5.23}$$

$$\Sigma_{12} - \dot{\sigma}^\star{}_{12} + \sigma_{11}^\star h_{21} \quad = \quad 0 \text{ at } x_2 = \pm h, \tag{5.24}$$

where

$$\sigma_{11}^\star = -\sigma_{22}^\star = -\frac{d_2^2}{2\varepsilon_0}, \qquad \dot{\sigma}^\star{}_{22} = \varepsilon_0 \dot{e}_2^\star e_2^\star, \qquad \dot{\sigma}^\star{}_{12} = \varepsilon_0 \dot{e}_1^\star e_2^\star. \tag{5.25}$$

The expressions for Σ_{22} and Σ_{12} are given in Eqs. (5.18)-(5.19). The external electric fields do not vanish in this path, and hence Eq. (3.9) assumes the form

$$\dot{d}_2^\star - \check{d}_2 + d_2^\star h_{22} \quad = \quad 0 \text{ at } x_2 = \pm h, \tag{5.26}$$

where $d_2^\star = d_2$. The remaining jump in Eq. (3.10) is

$$\dot{e}_1^\star - \check{e}_1 + e_2^\star h_{21} = 0 \text{ at } x_2 = \pm h. \tag{5.27}$$

Eqs. (5.16)-(5.22) and Eqs. (5.23)-(5.27) complete the necessary set of eight boundary conditions for the eight unknowns for paths A and B, and path C, respectively. Furthermore, they constitute a set of linear homogeneous equations in the unknowns, hence non-trivial solutions exist when the determinant of the coefficients matrix vanishes. This, in turn, is the extension of the well-known Rayleigh-Lamb transcendental equation for a purely elastic layer, and Tiersten's result for a piezoelectric plate (Tiersten, 1963a) within the framework of infinitesimal deformations. Of practical interest is the dependency of the dispersion relation, usually given in terms of the frequency spectrum, on the bias field and the finite deformation. These are discussed in the next section

6. Analysis of the dispersion relation

The working scheme of this section can be formulated as follows: *Given an angular frequency of excitation* ω, *we determine the associated wavenumbers* $\{k_m\}$ *satisfying the generalized transcendental equation, determine the velocities of the propagating waves* $c_m = \omega/k_m$, *and examine how these vary as functions of the bias field and pre-stretch.* Specifically, for paths A and C the dependency on the bias field is examined for a few representative values of $\hat{D}$. For path B, having the deformed configuration fixed we find it advantages to explore the dependency in terms of $\hat{d}$. Recalling that along this path the pre-stretch and the electric displacement field are independent, the dependency of the dispersion relation on a few representative values of the pre-stretch $\tilde{\lambda}$ is also examined. Of special interest is the identification and evaluation of the fundamental modes, i.e., those modes having finite velocity in the limit of long waves (e.g., Lutianov and Rogerson, 2010).

We find it useful to represent the results in terms of the dimensionless quantities $\hat{k} = hk$, $\hat{c} = c/c_B$ and $\hat{\omega} = \hat{c}\hat{k}$, where $c_B = \sqrt{\mu/\rho}$ is the bulk shear wave velocity in an isotropic elastic material. Further, our numerical investigation implies that the value of the parameter ε_r has only minor a influence on the frequency spectrum due to the choices $\hat{D} = D_2/\sqrt{\mu\varepsilon}$ and $\hat{d} = d_2/\sqrt{\mu\varepsilon}$ which are normalized by the material permittivity. Accordingly, as a representative value we chose $\varepsilon_r = 3$.

In their fundamental works Lord Rayleigh (1889) and Lamb (1889) had shown that in the purely elastic case a decomposition of the mechanical vibrations can be made into symmetric (extensional) and antisymmetric (flexural) modes with respect to the mid-plane of the layer. Interestingly, a similar decomposition of the mechanical displacement is possible for the coupled problem. Interestingly, it turns out that the symmetry of the electrical displacements is reversed in the sense that whenever the mechanical displacements are symmetric, the electrical displacements are antisymmetric, and vice versa. To distinguish between the two types of modes we employ the following procedure. For the antisymmetric modes we subtract Eq. (5.23) evaluated at $x_2 = -h$ from its value at $x_2 = h$, and similarly with Eq. (5.27). Subsequently, we add Eq. (5.24) evaluated at $x_2 = -h$ to its value at $x_2 = h$, and similarly with Eq. (5.26). We end up with a system of four homogeneous

equations in terms of the four constants

$$A_1^+ = A_1 + A_3, \quad A_5^+ = A_5 + A_6, \qquad B^- = B_3 - B_1, \quad C^+ = C_1 + C_2. \tag{6.1}$$

The dispersion relation derived from the determinant of this system provides the speed of propagation of waves associated with the antisymmetric modes. The symmetric modes can be derived by changing the foregoing operations. Thus, to add Eq. (5.23) evaluated at $x_2 = -h$ to its value at $x_2 = h$, and similarly with Eq. (5.27). Analogously, to subtract Eq. (5.24) evaluated at $x_2 = -h$ from its value at $x_2 = h$, and also with Eq. (5.26). These operations lead to system of four homogeneous equations in terms of the four constants

$$A_1^- = A_1 - A_3, \quad A_5^- = A_5 - A_6, \qquad B^+ = B_3 + B_1, \quad C^- = C_1 - C_2. \tag{6.2}$$

Path A: expansion-free finite loading. Fig. 6.1a displays the normalized velocity $\hat{c}$ as a function of the normalized wavenumber $\hat{k}$ for a few values of $\hat{D}$. Herein and henceforth the continuous and dashed curves correspond to the symmetric and antisymmetric modes, respectively. The markless curve, and the curves with triangle and circle marks correspond to $\hat{D} = 0, 1$ and 2, respectively. These values of the biased fields induce the principal stretches $\lambda = 1, 1.19$ and 1.49, respectively.

The case $\hat{D} = 0$ corresponds to the purely elastic problem. In this case the generalized solution recovers the classic Rayleigh-Lamb dispersion relation, as it should. Note that one can perceive variation in $\hat{k}$ as variation in the plate thickness for a fixed wavenumber. Thus, as $\hat{k}$ increases the plate geometry becomes similar to that of a half-space. Accordingly, the symmetric and the antisymmetric branches become closer, such that in the limit of $\hat{k} \to \infty$ they coincide and attain the surface wave velocity. In particular, the fundamental modes propagate at a velocity $\hat{c} = 0.955$ in the limit of short waves (large $\hat{k}$), which is the propagation velocity of Rayleigh surface waves. Further, the fundamental symmetric mode attains the well known result $\hat{c} = 2$ in the limit of long waves, or, equivalently, thin layers (small $\hat{k}$).

As $\hat{D}$ increases a monotonous rise of the velocity in the limit of long waves for the symmetric mode is revealed. The velocity at this limit can be derived analytically upon taking the first term in the Taylor series expansion of the symmetric dispersion relation in the neighborhood of $\hat{k} = 0$. Equating it to zero yields an explicit expression for the velocity in the limit of long waves, namely

$$\hat{c} = 2\left(1 + \hat{D}^2\right)^{1/4} = 2\lambda. \tag{6.3}$$

A monotonous rise of the velocity in the limit of short waves is observed too. We stress that the asymptotic values of the dimensionless speed are in agreement with the corresponding results obtained with an analysis of surface waves.

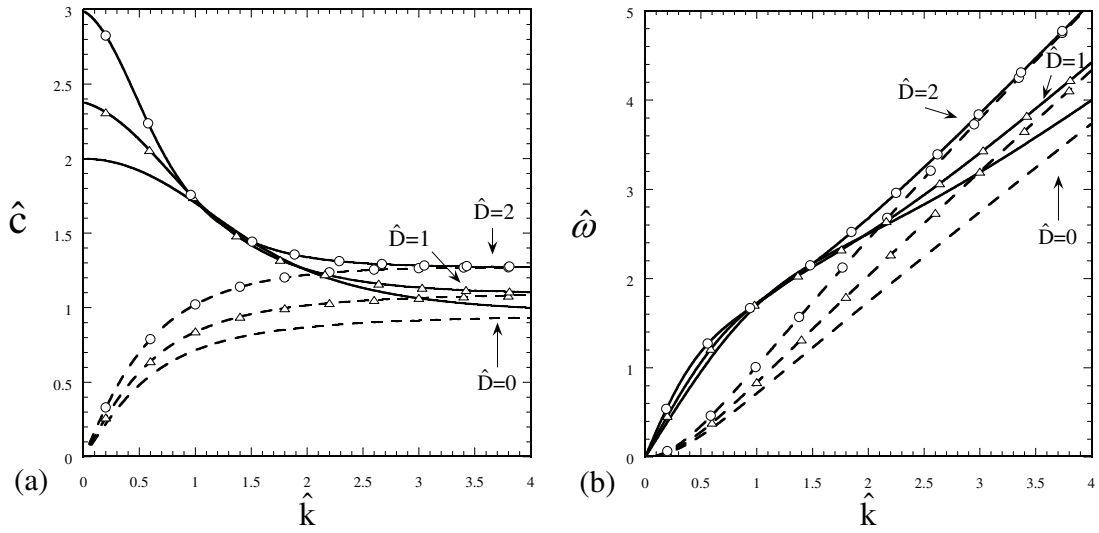

FIGURE 6.1. Path A: the normalized velocity $\hat{c}$ (a) and angular frequency $\hat{\omega}$ (b) as functions of the normalized wavenumber $\hat{k}$ for the expansion-free finite loading path. The continuous and dashed curves correspond to the symmetric and antisymmetric parts, respectively. The markless curve, and the curves with triangle and circle marks correspond to $\hat{D} = 0, 1$ and 2, respectively.

We find that all antisymmetric branches emerge at the origin, so that no loss of stability in terms of diffuse mode is identified, i.e., a vanishing $\hat{c}$ for non-zero wavenumbers. For this loading path a possible instability could be macroscopic instability associated with the loss of positive definiteness of the tangent constitutive operator (Zhao and Suo, 2007, Bertoldi and Gei, 2011) that however cannot occur for a DH layer with vanishing longitudinal stress.

Fig. 6.1b displays the normalized angular frequency $\hat{\omega}$ as function of the normalized wavenumber $\hat{k}$. We point out that the slope of the curves remains positive. Consequently, a unique wavenumber $\hat{k}$ is associated with each value of $\hat{\omega}$ along a specific curve. In other words, exciting the layer along this path with a certain frequency will give rise to a single wavelength of each fundamental mode, and increasing values of $\hat{\omega}$ will result in shorter waves.

Path B: Pre-stretched layer. Three representative types of pre-stretch where chosen, namely a tensile pre-stretch with $\tilde{\lambda} = 1.5$, no pre-stretch $\tilde{\lambda} = 1$ (the layer is clamped in its the reference configuration), and a pre-compression with $\tilde{\lambda} = 0.8$. We recall that here we find it useful to use

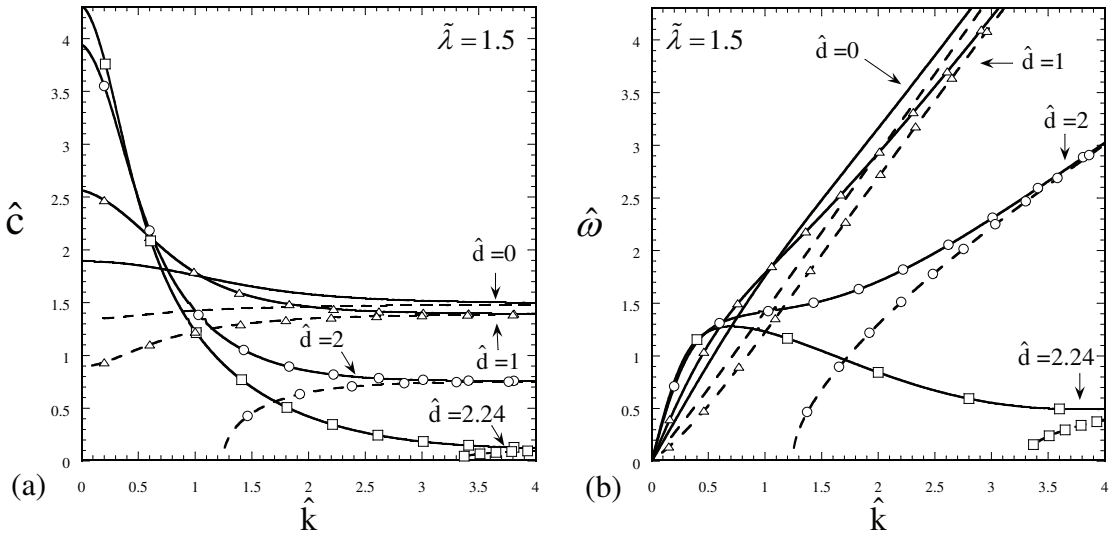

FIGURE 6.2. Path B: the normalized velocity $\hat{c}$ (a) and angular frequency $\hat{\omega}$ (b) as functions of the normalized wavenumber $\hat{k}$ for for $\tilde{\lambda}$=1.5. The continuous and dashed curves correspond to the symmetric and antisymmetric parts, respectively. The markless curve, and the curves with triangle, circle and square marks correspond to $\hat{d}=0,1,2$ and 2.24, respectively.

the current quantity $\hat{d}=d_2/\sqrt{\mu\varepsilon}$ as a measure for the bias field, as $\tilde{\lambda}$ is held fixed. Figs. 6.2a, 6.3a and 6.4a display the normalized velocity $\hat{c}$ as a function of the normalized wavenumber $\hat{k}$ for $\tilde{\lambda}=1.5,1$ and 0.8, respectively. The continuous and dashed curves correspond to the symmetric and antisymmetric parts, respectively. The markless curve, and the curves with triangle and circle marks correspond to $\hat{d}=0,1$ and 2, respectively. The curves with square marks correspond to $\hat{d}=2.24,1.75$ and 1.44 in Figs. 6.2-6.4, respectively.

With regard to the symmetric branches, the velocity in the limit of long waves increases with values of $\hat{d}$, in a manner similar to the one observed for path A. Here again we take the first term in the Taylor series expansion of the symmetric dispersion relation in the neighborhood of $\hat{k}=0$ and equate it to zero. The resulting explicit expression for the velocity in this limit is

$$\hat{c}=\sqrt{3\left(\hat{d}^2+\tilde{\lambda}^{-2}\right)+\tilde{\lambda}^2}. \tag{6.4}$$

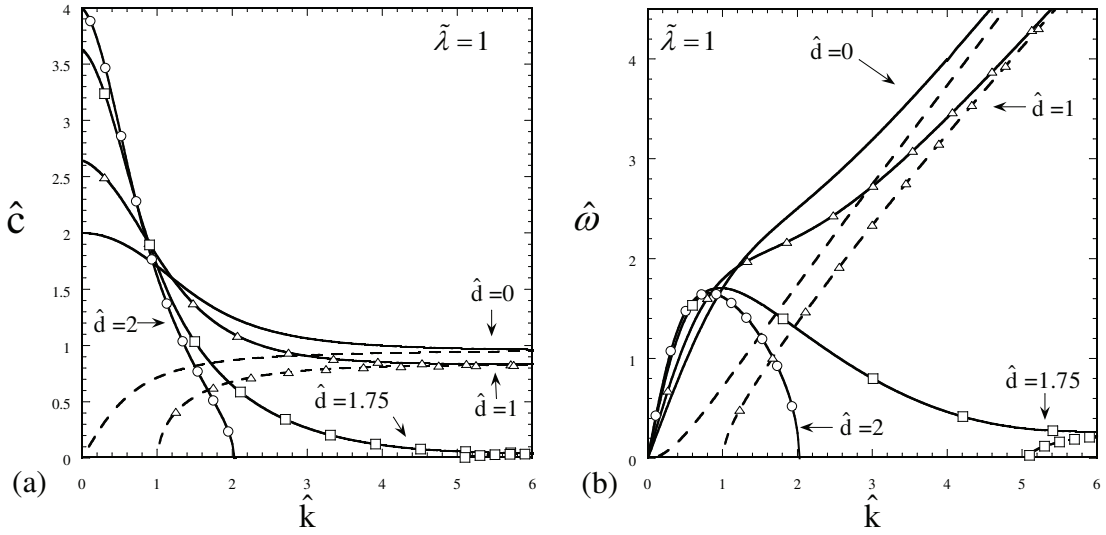

FIGURE 6.3. Path B: the normalized velocity $\hat{c}$ (a) and angular frequency $\hat{\omega}$ (b) as functions of the normalized wavenumber $\hat{k}$ for $\tilde{\lambda}$=1. The continuous and dashed curves correspond to the symmetric and antisymmetric parts, respectively. The markless curve, and the curves with triangle, square and circle marks correspond to $\hat{d} = 0, 1, 1.75$ and 2, respectively.

Interestingly, a reversed trend is revealed in the limit of short waves, such that the surface wave velocity decreases monotonically with $\hat{d}$, in contrast to the situation in path A. The difference stems from the emergence of compressive stress in path B, as the layer cannot elongate with increasing values of $\hat{d}$ due to the fixed boundary. The surface wave velocity decays until it reaches a vanishing value associated with a loss of surface stability. This is attained when a threshold value $\hat{d}_{th}$ is applied, such that

$$\lim_{\hat{k}\to\infty} \hat{c} = 0. \tag{6.5}$$

Thus $\hat{d}_{th}$ can be perceived as the value of $\hat{d}$ at which a half-space losses its stability. This threshold value depends on the pre-stretch such that it increases monotonically with $\tilde{\lambda}$, revealing a stabilizing effect of the pre-stretch. Specifically, for $\tilde{\lambda} = 1.5$, 1 and 0.8 we calculate numerically the values $\hat{d}_{th} = 2.245, 1.753$ and 1.453, respectively. When $\hat{d} > \hat{d}_{th}$ the velocity vanishes at a finite cutoff wavenumber which we denote by $\hat{k}_{co}^{sym}$. In a way $\hat{k}_{co}^{sym}$ defines a critical wavelength, beyond which no propagation of waves is exhibited. Further increase of $\hat{d}$ will result in smaller values of $\hat{k}_{co}^{sym}$. For

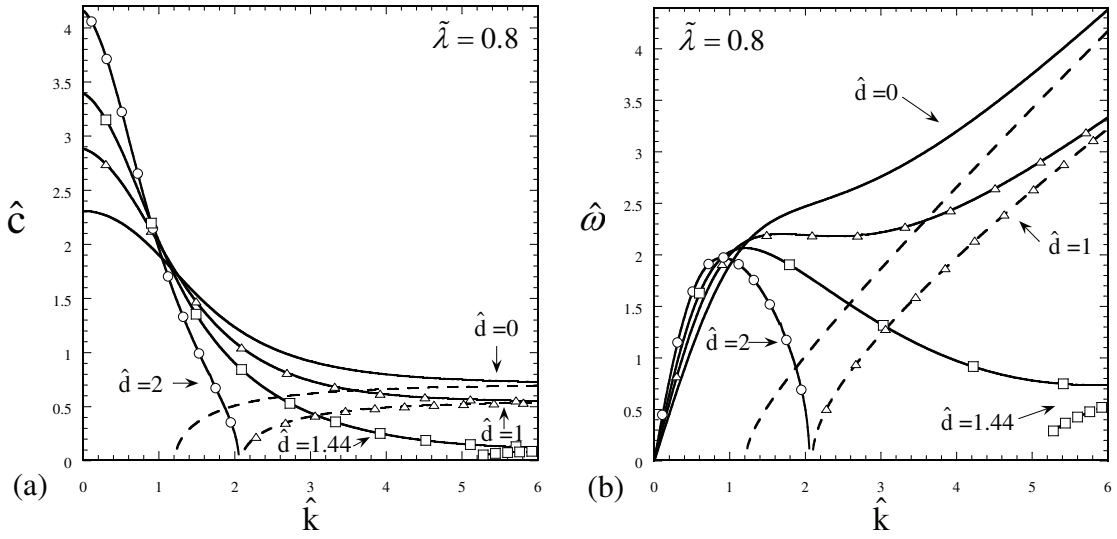

FIGURE 6.4. Path B: the normalized velocity $\hat{c}$ (a) and angular frequency $\hat{\omega}$ (b) as functions of the normalized wavenumber $\hat{k}$ for $\tilde{\lambda}$=0.8. The continuous and dashed curves correspond to the symmetric and antisymmetric parts, respectively. The markless curve, and the curves with triangle, square and circle marks correspond to $\hat{d} = 0, 1, 1.44$ and 2, respectively.

completeness, we note that our numerical investigation shows that for the case $\hat{d} = 0$ the solution recovers Biot's result for loss of stability under compression of a neo-Hookean half-space at a pre-compression of $\tilde{\lambda} = 0.544$.

Turning to the antisymmetric branches, we observe an essentially different evolution from the one in path A. Thus, in this case the branches emerge from various points. We denote the wavenumber at which the branch emerges by $\hat{k}_{co}^{anti}$. In a way $\hat{k}_{co}^{anti}$ defines a critical wavelength beneath which there is no stable propagation of longer waves. The value of $\hat{k}_{co}^{anti}$ increases when $\hat{d}$ is increased, up to the threshold value $\hat{d}_{th}$, at which $\hat{k}_{co}^{anti}$ tends to infinity. We stress that $\hat{d}_{th}$ is the one satisfying Eq. (6.5) as expected, since in the limit of half-space the two branches coincide.

Figs. 6.2b, 6.3b, and 6.4b display the dispersion relation in terms of the normalized frequency $\hat{\omega}$ as a function of the normalized wavenumber $\hat{k}$, with identical legend to the one previously used. It is observed how, unlike the corresponding curves in path A, for some values of $\hat{d}$ the symmetric curves are not monotonous. In some cases the slope of the curves is changing from positive to negative and to positive once again. This corresponds to a situation where for the same frequency there

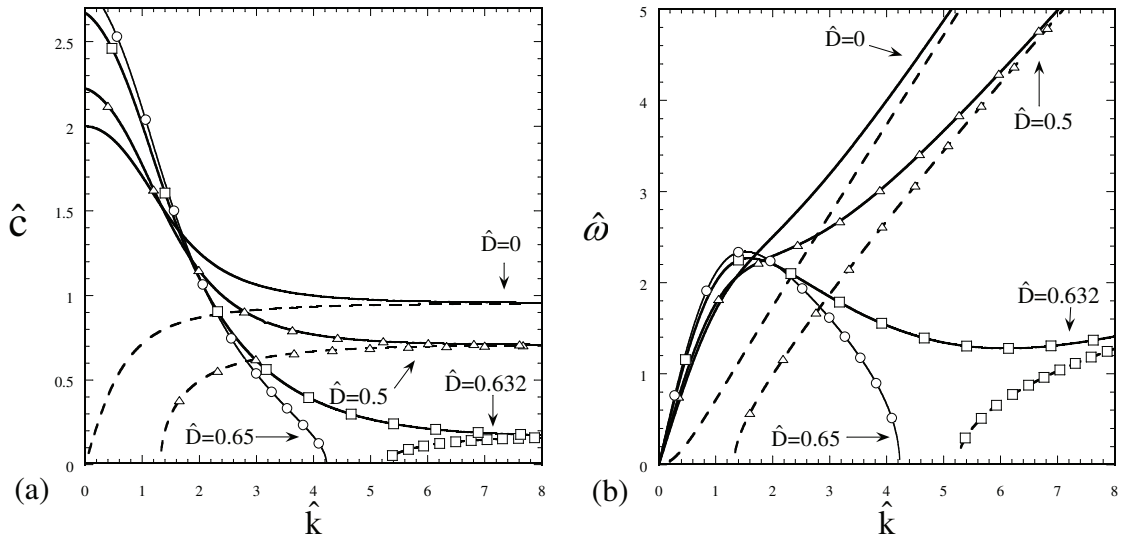

FIGURE 6.5. Path C: the normalized velocity $\hat{c}$ (a) and angular frequency $\hat{\omega}$ (b) as functions of the normalized wavenumber $\hat{k}$ for a layer immersed in an electric field. The continuous and dashed curves correspond to the symmetric and antisymmetric parts, respectively. The markless curve, and the curves with triangle, circle and square marks correspond to $\hat{D} = 0, 0.5, 0.632$ and 0.65, respectively.

are more than one wavenumber satisfying the dispersion relation for the fundamental symmetric mode, and subsequently the pertained different wavelengths propagate with different velocities. If the frequency is to be taken as the independent variable, this suggests a peculiar phenomenon in which as the frequency is increased there is a possibility for the appearance of shorter and slower waves that propagate along with the "primary" waves.

Path C: A layer immersed in an electric fields. We recall that Eq. (4.13a) states that the layer expands along the direction of the electric displacement, in a manner opposite to the one revealed in paths A and B. Further, the stretch depends strongly on the material permittivity, even when the normalized quantity $\hat{D}$ is used. For the choice $\varepsilon_r = 3$ the maximal value of admissible $\hat{D}$ is $1/\sqrt{2}$, as λ vanishes for this value in view of Eq. (4.13a). Consequently, the values of $\hat{D}$ considered in path A cannot be used, and even values of $\hat{D}$ that result in the same values of λ are not feasible as here $\lambda < 1$, whereas along path A $\lambda > 1$. Nonetheless, attempting to investigate cases analogue

to those addressed in path A, we choose values of $\hat{D}$ that yield values of $\max\{\lambda, 1/\lambda\}$ similar to those considered in path A.

Fig. 6.5a displays the normalized velocity $\hat{c}$ as a function of the normalized wavenumber $\hat{k}$ for $\hat{D} = 0, 0.5, 0.632$ and 0.65. These values correspond to principle maximal stretche ratios $1, 1.2, 1.5$ and 1.59, respectively. The continuous and dashed curves correspond to the symmetric and antisymmetric solutions, respectively. The markless curve, and the curves with triangle, circle and square marks correspond to $\hat{D} = 0, 0.5, 0.632$ and 0.65, respectively. Once again, the symmetric modes exhibit a rise in the velocity in the limit of long waves with increasing values of $\hat{D}$. In a manner similar to path B, the trend is reversed in the short waves limit, and the surface wave velocity decreases monotonically as $\hat{D}$ increases. This is a consequence of the resultant compressive stress that can be determined by substitution of Eq. (5.25a) into Eq. (2.4a) for the jump in the stress. Thus, the surface wave velocity decays as a function of $\hat{D}$, until it reaches a vanishing value associated with a loss of surface stability, i.e., satisfying Eq. (6.5). Once again we denote the threshold value of $\hat{D}$ for which the latter holds by $\hat{D}_{th}$. In this numerical example we find that $\hat{D}_{th} = 0.636$. As in Path B, when $\hat{D} > \hat{D}_{th}$ the velocity of the symmetric modes vanishes at a finite cutoff wavenumber $\hat{k}_{co}^{sym}$ beyond which no shorter waves are exhibited.

The behavior of the antisymmetric modes is also reminiscent of the one observed for path B. Specifically, it is observed how the curves emerge at different cutoff wavenumbers $\hat{k}_{co}^{anti}$ defining critical wavelength beneath which there is no stable propagation of longer waves. The cutoff wavenumber increases monotonically with values of $\hat{D}$, and reaches infinity when $\hat{D}$ attains the aforementioned value $\hat{D}_{th}$. Subsequently, when $\hat{D} > \hat{D}_{th}$ there is no stable antisymmetric wave propagation.

Fig. 6.5b displays the dispersion relation in terms of the normalized frequency $\hat{\omega}$ as function of the normalized wavenumber $\hat{k}$. Trends similar to the ones observed in path B are revealed. In particular, the monotonicity is lost when $\hat{D} > 0.584$, where the positive slop of the curve becomes negative and then positive again. Here again, this implies that imposing certain frequencies may yield more than one wavelength of the fundamental symmetric mode satisfying the dispersion relation. In turn, this suggests that when the frequency is increased there is a possibility of simultaneous different phase velocities.

7. Concluding remarks

In view of the emergence of modern EAPs capable of large deformations in response to electric excitation we examine the topic of small waves propagation superposed on finitely deformed dielectric elastomer layers. Specifically, we considered a layer whose electromechanical behavior is characterized by the DH model when subjected to a coaxial finite deformation. Three different

loading paths which result in the aforementioned finite configurations were addressed. In path A the layer is free to expand along its longitudinal direction and deformed due to the electric excitation along its thickness. In path B the layer is initially pre-stretched, then clamped, and subsequently the electric field is employed. In path C the layer is immersed in a pre-existing electric field.

Following Dorfmann and Ogden (2010) small perturbations on top of the homogeneous finite deformation are considered. The coupled equations of incremental electrodynamics along with the pertained boundary conditions yielded the desired dispersion relation. For the DH model this required a non-conventional presentation of the solution of the governing equations. It was shown that a separation of the mechanical and electric waves to symmetric and antisymmetric modes with respect to the mid-plane of the layer is feasible. We find that the symmetric mechanical waves are accompanied by antisymmetric electric waves and vice versa.

Numerical investigation of the fundamental modes was conducted to examine the influence of the bias field along the three loading paths. For path B we also examined the effect of pre-stretch. In path A the velocity of both short waves (half-space, large $\hat{k}$) and long waves (thin plate, small $\hat{k}$) is increased when the electric displacement field is enhanced. While in the limit of long waves a similar rise in the velocity is observed in path B, the velocity decreases as function of the electric displacement field in the limit of short waves. The existence of a threshold values of $\hat{d}$ at which the layer losses stability is observed. The pre-stretch effect is shown to be stabilizing, as higher values of $\hat{d}$ are needed to reach the onset of instability. Dispersion relations similar to the ones obtained in path B were observed in path C. We finally stress that along all paths there is a marked influence of the bias electric field and pre-stretch on the propagation speed. This phenomenon lends itself as a possible control mechanism for the speed of the waves, or even for filtering specific wavelengths with suitable adjustment of the bias field and pre-stretch.

ACKNOWLEDGEMENTS

The first author wishes to thank a scholarship in the framework of the Erasmus Mundus External Cooperation Window (grant lot3.emecw.com). The second author gratefully acknowledges the financial support of COST Action MP1003 "European Scientific Network for Artificial Muscles".

REFERENCES

Bar-Cohen, Y. (2002). Electroactive polymers as artificial muscles, *J. of Spacecraft and Rockets* **39**: 822–827.

Bertoldi, K. and Gei, M. (2011). Instabilities in multilayered soft dielectrics, *Journal of the Mechanics and Physics of Solids* **59**(1): 18 – 42.

Bustamante, R., Dorfmann, A. and Ogden, R. (2009). Nonlinear electroelastostatics: a variational framework, *Zeitschrift für Angewandte Mathematik und Physik* **60**: 154–177.

Carpi, F. and Smela, E. (2009). *Biomedical Applications of Elecroactive Polymer Actuators*, John Wiley & Sons Ltd., Chichester, UK.

deBotton, G., Tevet-Deree, L. and Socolsky, E. A. (2007). Electroactive heterogeneous polymers: analysis and applications to laminated composites, *Mechanics of Advanced Materials and Structures* **14**: 13–22.

Dorfmann, A. and Ogden, R. W. (2005). Nonlinear electroelasticity, *Acta. Mech.* **174**: 167–183.

Dorfmann, A. and Ogden, R. W. (2010). Electroelastic waves in a finitely deformed electroactive material, *IMA J Appl Math* **75**: 603–636.

Ericksen, J. L. (2007). Theory of elastic dielectrics revisited, *Archive for Rational Mechanics and Analysis* **183**: 299–313.

Eringen, A. C. (1963). On the foundations of electroelastostatics, *Int. J. Engng. Sci.* **1**: 127–153.

Eringen, A. C. and Maugin, G. A. (1990). *Electrodynamics of Continua, vol. I*, Springer, New York.

Kofod, G. (2008). The static actuation of dielectric elastomer actuators: how does pre-stretch improve actuation?, *Journal of Physics D: Applied Physics* **41**(21): 215405.

Kovetz, A. (2000). *Electromagnetic Theory*, Oxford University Press.

Lamb, H. (1889). On the flexure of an elastic plate, *Proc. Lond. math. Soc.* **21**: 70–90.

Lutianov, M. and Rogerson, G. A. (2010). The influence of boundary conditions on dispersion in an elastic plate, *Mechanics Research Communications* **37**(2): 219 – 224.

McMeeking, R. M. and Landis, C. M. (2005). Electrostatic forces and stored energy for deformable dielectric materials, *J. Appl. Mech., Trans. ASME* **72**: 581–590.

Mockensturm, E. M. and Goulbourne, N. (2006). Dynamic response of dielectric elastomers, *Int. J. Nonlinear Mech.* **41**: 388 – 395.

Pelrine, R., Kornbluh, R., Pei, Q.-B. and Joseph, J. (2000). High-speed electrically actuated elastomers with strain greater than 100%, *Science* **287**: 836–839.

Plante, J. S. and Dubowsky, S. (2006). Large-scale failure modes of dielectric elastomer actuators, *International Journal of Solids and Structures* **43**(25-26): 7727 – 7751.

Rayleigh, J. W. S. (1887). On waves propagated along the plane surface of an elastic solid, *Proc. Lond. math. Soc.* **17**: 4–11.

Rayleigh, L. (1889). On the free vibrations of an infinite plate of homogeneous isotropic elastic matter, *Proceedings of the London Mathematical Society* **s1-20**: 225–234.

Suo, Z., Zhao, X. and Greene, W. H. (2008). A nonlinear field theory of deformable dielectrics, *J. Mech. Phys. Solids* **56**(2): 467–486.

Tiersten, H. F. (1963a). Thickness vibrations of piezoelectric plates, *The Journal of the Acoustical Society of America* **35**(1): 53–58.

Tiersten, H. F. (1963b). Wave propagation in an infinite piezoelectric plate, *The Journal of the Acoustical Society of America* **35**(2): 234–239.

Toupin, R. A. (1956). The elastic dielectric, *Arch. Rational. Mech. Anal.* **5**: 849–915.

Toupin, R. A. (1963). A dynamical theory of elastic dielectrics, *International Journal of Engineering Science* **1**(1): 101 – 126.

Yang, J. and Hu, Y. (2004). Mechanics of electroelastic bodies under biasing fields, *Applied Mechanics Reviews* **57**(3): 173–189.

Zhao, X. and Suo, Z. (2007). Method to analyze electromechanical stability of dielectric elastomers, *Appl. Phys. Lett.*

Zhu, J., Cai, S. and Suo, Z. (2010). Nonlinear oscillation of a dielectric elastomer balloon, *Polymer International* **59**(3): 378–383.